15th AIAA/CEAS Aeroacoustics Conference (30th AIAA Aeroacoustics Conference)
11 - 13 May 2009, Miami, Florida

AIAA 2009-3395

Properties of the Lattice–Boltzmann Method for Acoustics

Guillaume A. Brès*, Franck Pérot†, and David Freed‡
Exa Corporation, Brisbane, CA 94005, U.S.A.

Numerical simulations are performed to investigate the fundamental acoustics properties of the Lattice–Boltzmann method. The propagation of planar acoustic waves is studied to determine the resolution dependence of numerical dissipation and dispersion. The two setups considered correspond to the temporal decay of a standing plane wave in a periodic domain, and the spatial decay of a propagating planar acoustic pulse of Gaussian shape. Theoretical dispersion relations are obtained from the corresponding temporal and spatial analyses of the linearized Navier–Stokes equations. Comparison of theoretical and numerical predictions show good agreement and demonstrate the low dispersive and dissipative capabilities the Lattice–Boltzmann method. The analysis is performed with and without turbulence modeling, and the changes in dissipation and dispersion are discussed. Overall, the results show that the Lattice–Boltzmann method can accurately reproduce time-explicit acoustic phenomena.

Nomenclature

a_S	Absorptive loss in dB/m
a_λ	Absorptive loss in dB per λ
$a_{\Delta x}$	Absorptive loss in dB per Δx
c	Speed of sound
c_S, c_T	Phase speed
C_g	Group speed
f	Frequency
I	Acoustic Intensity
k	Wavenumber
N_{ppw}	Number of points per wavelength
P	Pressure
T	Temperature
t	Time
u, v, w	Cartesian velocity components
x, y, z	Cartesian coordinates
α_S, α_T	Dissipation rate
Δx	Grid size
λ	Wavelength of acoustic wave
μ	Dynamic viscosity
ν	Kinematic viscosity
ρ	Density
σ	Gaussian pulse width
τ	LBM relaxation time
τ_S	Acoustic relaxation time, $\tau_S = 2\nu/c_0^2$
ω	Angular frequency

Superscript

^{num}	Numerical deviation
$'$	Perturbation quantity
$\hat{}$	Complex value

Subscript

0	Ambient property
S	Quantity for spatial analysis
T	Quantity for temporal analysis

I. Introduction

The Lattice–Boltzmann method (LBM) is a well-known computational fluid dynamics (CFD) method that models flow in a way that is consistent with formal solutions of the transient, viscous and compressible Navier–Stokes equations.[1–3] The Lattice–Boltzmann scheme together with the very large eddy turbulence model was shown to accurately capture the aerodynamics of high Reynolds number flows,[4,5] as well as

*Aeroacoustics Engineer, gbres@exa.com, member AIAA
†Principal Aeroacoustics Engineer, perot@exa.com, member AIAA
‡Director of Aeroacoustics Applications, dmfreed@exa.com

turbulent wall pressure fluctuations due to separated and reattached flows.[6–8] As a result, LBM is now being widely used as an investigative and prediction tool for practical engineering applications in the automobile[9–13] and aerospace[14,15] industries.

In contrast, the use of LBM for acoustics is fairly recent and more limited. Sound wave propagation using LBM was first studied by Buick *et al.*[16] (without viscosity) and then Dellar[17] (with the presence of viscosity), both with satisfactory results. Crouse *et al.*[18] used LBM to investigate four canonical acoustic problems involving traveling and standing acoustic waves. The first two test cases examined the propagation of acoustic waves in one and two dimensions, while the other two cases dealt with acoutic resonance. Their results showed the basic capability of the LBM to correctly reproduce fundamental acoustic phenomena. More recently, Marié *et al.*[19] estimated the dissipation and dispersion of acoustic waves for different Lattice–Boltzmann models and compared the results to various Navier–Stokes solvers. As the performance of their LBM solver was estimated between a second order and an optimized third order scheme in space (with three-step Runge-Kutta in time), their analysis again highlights the low dissipative capabilies of the Lattice-Boltzmann method.

The goal of the present work is to extend the previous studies on LBM, to fully address the requirements for accurate prediction of acoustics in real engineering applications such as fan noise and heat-ventilation-air conditioning (HVAC) systems. As the Lattice–Boltzmann method is already used to correctly model the flow field and flow-induced noise sources in these applications, the objective here is to demonstrate that it can also resolve directly the acoustic near-field (i.e., up to about 1 m from the sources), at no or marginal additional computational cost.

First, the temporal and spatial analyses of the linearized Navier–Stokes equations are carried out to obtain theoretical dispersion and dissipation relations for the propagation of a plane wave. Numerical simulations of a standing plane wave in periodic domain, and of a propagating planar acoustic pulse of Gaussian shape, are then performed, for both the DNS and turbulent version of the code. The results are compared to theoretical predictions to evaluate numerical dissipation and dispersion as a function of resolution.

II. Theoretical formulation

A. Numerical methods

The CFD code PowerFLOW 4.0d based on the Lattice–Boltzmann method is used in this study. Unlike traditional methods solving the discretized Navier–Stokes equations on a computation grid, the LBM approach focuses on the mesoscopic scales via the discrete Boltzmann equation. That is, instead of studying the global behavior of a fluid, LBM tracks the statistical displacement of groups of particles and deducts the macroscopic scale behavior by evolving the particle distribution on a lattice.

The method is briefly reviewed here. The starting point is the distribution function F_i expressing the probability of presence of particles at position $\mathbf{x}$ and discrete velocity ξ_i at time t. The Lattice–Boltzmann equation is typically written in the following form:[20]

$$F_i(\mathbf{x}+\xi_i\Delta t, t+\Delta t) - F_i(\mathbf{x},t) = \frac{\Delta t}{\tau}\left[F_i^{eq}(\mathbf{x},t) - F_i(\mathbf{x},t)\right]. \tag{1}$$

The left-hand side of equation (1) corresponds to the particle advection, while the right-hand side is the collision term, representing relaxation (i.e., interaction of the particles). The well-known BGK approximation[21] is used to compute the local equilibrium distribution function $F_i^{eq}(\mathbf{x},t)$. The definition of the relaxation time τ is related to the kinematic viscosity and temperature by:

$$\tau = \frac{\nu}{T} + \frac{\Delta t}{2}. \tag{2}$$

The macroscopic quantities, density ρ and momentum density $\rho\mathbf{u}$, are determined directly from the distribution function F_i, using the moment summations:

$$\rho(\mathbf{x},t) = \sum_i F_i(\mathbf{x},t), \qquad \rho\mathbf{u}(\mathbf{x},t) = \sum_i F_i(\mathbf{x},t)\xi_i. \tag{3}$$

The full compressible viscous Navier–Stokes equations can be recovered from the Lattice–Boltzmann equation, using a multi-scale analysis,[22] for wavelengths $\lambda \gg \Delta x$ and frequencies $f \ll \Delta t$. The resulting

equation of state is that of an ideal gas, in the form $P = \rho T$. Therefore, LBM also inherently recovers acoustics.

The numerical scheme is solved on a grid composed of cubic volumetric elements called voxels, and variable resolution (VR) is allowed, where the grid size changes by a factor of two for adjacent resolution regions. The local computational nature of LBM allows for excellent parallelization, and the method is well adapted to handle complex arbitrary geometries.

Together with the definition of F_i^{eq}, equations (1) and (2) constitute the LBM scheme used to perform direct numerical simulations (DNS). For high Reynolds number simulations, turbulence modeling is incorported into the Lattice–Boltzmann equations by replacing the relaxation time by an effective turbulent relaxation time scale in equation (2). Additional details on the LBM numerical schemes, and the use of wall boundary conditions and turbulence modeling can be found in Refs. 23–26.

B. Acoustic plane wave solutions

The goal of the present study is to quantify the acoustic capabilities of the LBM approach, in particular in terms of dispersion (change in propagation speed) and dissipation (change in amplitude) of acoustic waves. To do so, we consider the propagation of small isothermal perturbations of the form $P = P_0 + P'$, with $P' \ll P_0$, in an ideal fluid at rest (i.e., $\mathbf{u} = \mathbf{u}'$). The linearized form of the three-dimensional Navier–Stokes equations that govern the propagation of sound waves can be reduced to a lossy wave equation[27,28]

$$\left(c_0^2 + \left[\frac{4}{3}\nu + \nu_B\right]\frac{\partial}{\partial t}\right)\nabla^2 P' = \frac{\partial^2 P'}{\partial t^2}, \tag{4}$$

where c_0 is the thermodynamic speed of sound in the ambient fluid, $\nu = \mu/\rho_0$ and $\nu_B = \mu_B/\rho_0$ are the kinematic shear and bulk viscosity, respectively. For the LBM-BGK isothermal model, the kinematic bulk viscosity has been shown to be $\nu_B = 2\nu/3$,[17] such that the effective viscosity modeled is $4\nu/3 + \nu_B = 2\nu$.

The plane wave $P' = \hat{A}\exp[i(\hat{k}x - \hat{\omega}t)]$ solutions of equation (4) now satisfy the dispersion relation

$$\left(c_0^2 - i\hat{\omega}2\nu\right)\hat{k}^2 = \hat{\omega}^2. \tag{5}$$

where $\hat{A}$, $\hat{k}$, and $\hat{\omega}$ are complex values. Solutions of the dispersion relation can be expressed using either a temporal or spatial approach, as described in the following sections.

1. *Temporal analysis*

In the temporal approach, the wavenumber $\hat{k} = k$ is real and prescribed, and equation (5) leads to a classical eigenvalue problem, solved for the complex angular frequency $\hat{\omega}$. In practice, this approach evaluates the change in frequency and decay in time of a plane wave of fixed wavelength (e.g., evolution of a standing acoustic wave)

The analytical solutions[19] take the form $\hat{\omega} = -ik^2\nu \pm kc_o\sqrt{1-(k\nu/c_0)^2}$. Restricting our attention to the wave traveling in the $+x$-direction, the solutions are therefore acoustic modes propagating with the phase speed $c_T = Re(\hat{\omega})/k$ and temporal dissipation rate $\alpha_T = -Im(\hat{\omega})$ given by

$$P' = \hat{A}\exp(-\alpha_T t)\exp[ik(x - c_T t)], \tag{6}$$

$$c_T = c_o\sqrt{1-\left(\frac{k\nu}{c_0}\right)^2}, \qquad \alpha_T = k^2\nu. \tag{7}$$

2. *Spatial analysis*

In the temporal approach, $\hat{\omega} = \omega$ is real and prescribed, and equation (5) is solved for the complex wavenumber $\hat{k}$, namely $\hat{k} = \pm\omega/\sqrt{c_0^2 - i\omega 2\nu}$. Here, this approach evaluates the change in wavelength and decay in space of a plane wave of fixed frequency (e.g., evolution of a propagating acoustic wave).

For the plane wave traveling in the $+x$-direction, the phase speed $c_S = \omega/Re(\hat{k})$ and spatial dissipation rate $\alpha_S = Im(\hat{k})$ can then be expressed[27] such that

$$P' = \hat{A}\exp(-\alpha_S x)\exp[i\omega(x/c_S - t)] \tag{8}$$

$$c_S = \sqrt{2}c_0\sqrt{\frac{1+(\omega\tau_S)^2}{\sqrt{1+(\omega\tau_S)^2}+1}}, \qquad \alpha_S = \frac{\omega}{\sqrt{2}c_0}\sqrt{\frac{\sqrt{1+(\omega\tau_S)^2}-1}{1+(\omega\tau_S)^2}}. \tag{9}$$

where $\tau_S = 2\nu/c_0^2$. Starting from equation (8), the decay in intensity level I with distance of propagation of the plane wave can be estimated by[27] $I(x) = I(0)\exp(-2\alpha_S x)$. The spatial absorptive loss a_S, expressed in dB/m, is then given by

$$a_S = \frac{1}{x}10\log\left[\frac{I(0)}{I(x)}\right] = \frac{20\alpha_S}{\ln(10)} \approx 8.7\alpha_S \tag{10}$$

Equation 10 can be used to estimate the loss in dB from physical (and numerical) dissipation for plane waves. This expression is still relevant in pratical case with spherically symmetric acoustic wave since the loss in intensity level with distance r is approximately[27] $20\log(r) + a_S r$.

3. Gaster transformation

To a first approximation, the spatial and temporal formulation can be related using Gaster transformation.[29] In this approach, the wavenumber and angular velocity are assumed to be analytic functions $\hat{k} = \hat{k}(\hat{\omega})$, and $\hat{\omega} = \hat{\omega}(\hat{k})$ in the complex plane, and their derivatives to be small. By integrating the Cauchy-Riemann relations, and neglecting higher order terms, it can be shown that if $Re(\hat{\omega}_{spatial}) \approx Re(\hat{\omega}_{temporal})$ (or $Re(\hat{k}_{spatial}) \approx Re(\hat{k}_{temporal})$) is explicitly chosen, then $Re(\hat{k}_{spatial}) \approx Re(\hat{k}_{temporal})$ (or $Re(\hat{\omega}_{spatial}) \approx Re(\hat{\omega}_{temporal})$), and the temporal and spatial dissipation rates satisfy

$$\frac{\alpha_T}{\alpha_S} = C_g, \qquad C_g = \frac{\partial Re(\hat{\omega})}{\partial Re(\hat{k})} \tag{11}$$

where C_g is the group velocity.

This approach can be applied in our case to yield useful approximations. For typical fluids (i.e., $\nu \approx 1.5\ 10^{-5}$ m^2/s, $c_0 \approx 343$ m/s) and frequencies relevant to acoustics (i.e., $f = \omega/2\pi$ up to 20 kHz), the terms $\omega\tau$ and $k\nu/c_o$ are small, of the order of 10^{-5}. Therefore, under the assumptions $\omega\tau \ll 1$ and $k\nu/c_o \ll 1$, equations (7) and (9) can be expanded to first order to give

$$c_T \approx c_o, \qquad \alpha_T = k^2\nu, \qquad c_S \approx c_0, \qquad \alpha_S \approx \frac{\omega}{2c_0}\omega\tau_S = \frac{\omega^2}{c_0^2}\frac{\nu}{c_0}. \tag{12}$$

In the process, the results of the Gaster transformation are recovered, namely that the phase speeds in the temporal and spatial formulations are identical (i.e., $k = \omega/c_0$) and that the dissipation rates are related by the group velocity $C_g = \partial\omega/\partial k = c_0$ (i.e., $\alpha_S = \alpha_T/c_0$).

III. Numerical setup

Numerical simulations are preformed to quantify the dispersion and dissipation of acoustic waves. The difference between the measured values and the theoretical predictions is interpreted as a deviation due to the numerical scheme, and is labeled with a superscript ^{num}. The two different setups are considered, corresponding to the temporal and spatial approaches previously described.

A. Planar standing wave

For this configuration (setup 1), a standing plane acoustic wave in a periodic domain without external flow is considered. The grid (voxel) size Δx is constant and the computational domain size is (λ, $5\Delta x$, $5\Delta x$). The initial condition is ($P_0 + P'$,$\rho_0 + \rho'$,u',v',w') given by:

$$P'(x,y,z,0) = A\sin\left(\frac{2\pi x}{\lambda}\right), \qquad \rho' = \frac{P'}{c_0^2}, \qquad u' = \frac{P'}{\rho_0 c_0}, \qquad v' = w' = 0,$$

where the perturbation amplitude $A = 10^{-3}\ P_0$ is small compare to P_0 to ensure linear acoustics. The simulation time is fixed to 50 periods, which is sufficient to estimate dispersion and dissipation effects.

This particular setup corresponds to a temporal analysis, since the numerical domain has a fixed dimension in terms of wavelength (i.e., $k = 2\pi/\lambda$ prescribed). Therefore, following equation (6) and the analysis described in the previous section, the acoustic pressure at time t is expected to be of the form

$$P'(x, y, z, t) = A \exp[-(\alpha_T + \alpha_T^{num})t] \sin[k(x - (c_T + c_T^{num})t)], \tag{13}$$

where c_T^{num} and α_T^{num} are the variation in phase speed and temporal dissipation rate due to the numerical scheme, respectively. These coefficients can be extrated from the time signal (see figure 1) at any location using a simple least-square fitting and the (physical) anticipated values c_T and α_T from equation (7). The results can either be expressed as a function of the number of points per wavelength $N_{ppw} = \lambda/\Delta x$, or the nondimensional wavenumber $k\Delta x = 2\pi/N_{ppw}$.

B. Planar pulse propagation

The second configuration (setup 2) corresponds to a spatial analysis representative of most practical cases, where a superposition of acoustic waves of fixed frequencies (i.e., superposition of ω prescribed) propagates through a numerical mesh of a given voxel size, such that each wave has a different number of points per wavelength.

For this setup, the plane wave is replaced by a planar pulse of Gaussian shape initially located at the origin:

$$P'(x, y, z, 0) = A \exp\left(-ln(2)\frac{x^2}{\sigma^2}\right), \qquad \rho' = \frac{P'}{c_0^2}, \qquad u' = \frac{P'}{\rho_0 c_0}, \qquad v' = w' = 0,$$

where $\sigma = 0.01$ m is the initial width of the pulse, and $A = 10^{-3}\ P_0$. The grid size Δx is constant and uniform throughout the computational domain and the boundary conditions are periodic in all three directions. Unlike setup 1, the domain size is fixed to 300σ in the x-direction, and the time-history of the fluid properties are recorded every 10σ between $x = 0$ and $x = 100\sigma$. The simulation time is limited to one pulse passage, to avoid contamination of the signal by any transient or boundary condition effects.

The pulse signal in the time domain (see figure 3) is then transformed into a linear combination of acoustic waves of different frequencies in Fourier space. This choice of initial condition (rather than plane monochromatic acoustic waves) yields the complete frequency dependence of the dispersion and dissipation in only one simulation. The pressure time-history at a reference position (say $x = 0$) and the propagated signals at any distance x are therefore expanded into Fourier integrals:

$$\begin{aligned} P'(0, t) &= \frac{1}{\sqrt{2\pi}} \int_{-\infty}^{+\infty} \hat{P}'(0, \omega) e^{-i\omega t} d\omega, \\ P'(x, t) &= \frac{1}{\sqrt{2\pi}} \int_{-\infty}^{+\infty} \hat{P}'(x, \omega) e^{-i\omega t} d\omega \end{aligned} \tag{14}$$

Here, the spatial dependence of the Fourier coefficient of pressure $\hat{P}'(x, \omega)$ is of the same form as in equation (8), that is

$$\hat{P}'(x, \omega) = \hat{P}'(0, \omega) \exp[-(\alpha_S + \alpha_S^{num})x] \exp[i\omega \frac{x}{c_S + c_s^{num}}], \tag{15}$$

where c_S^{num} and α_S^{num} are the variation in phase speed and spatial dissipation rate due to numerical scheme, respectively. Given the (physical) expected values from equation (9), these coefficients can therefore be estimated as a function of frequency from the phase and amplitude of the ratio $\hat{P}'(x, \omega)/\hat{P}'(0, \omega)$, for a given spatial resolution.

The initial pulse width σ was chosen to ensure that the results reported with this method were independent of its actual value. A preliminary study showed that $\sigma = 0.01$ m was sufficient to accurately capture the variations in phase speed and spatial dissipation, for the range of resolution and frequency of interest.

IV. Results and discussion

A. DNS code

First, the DNS version of the LBM code is used to study the accuracy of the direct numerical simulations. For the results presented in this section, the viscosity is set to $\nu = 1.5\ 10^{-2}$ m^2/s.

Figure 1 shows the acoustic pressure time-history for the sine wave in a periodic domain, corresponding to setup 1, with $N_{ppw} = 12$ points per wavelength. For this result, the dimension of the domain was set to one wavelength for a signal of frequency $f = 10$ kHz. A parametric study on the resolution (i.e., the number of points per wavelength) was performed, and different frequencies and values for viscosity were also considered. As expected, the results are only a function of N_{ppw}, and independent of f and ν in our range of interest.

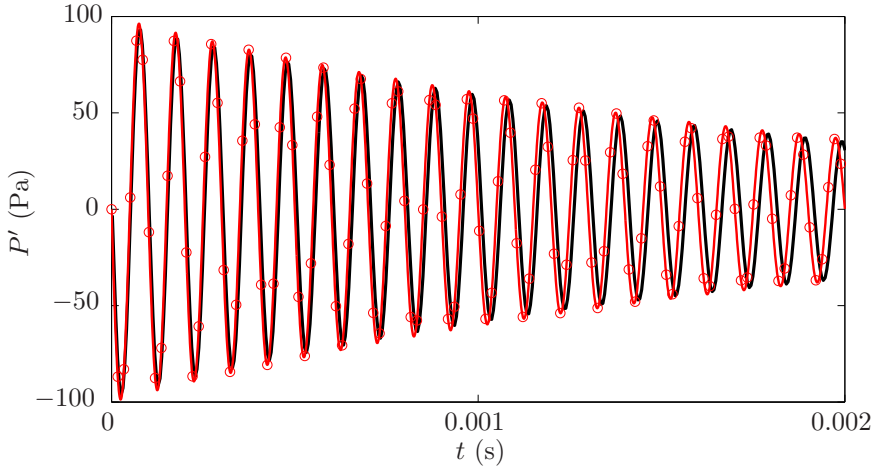

Figure 1. Acoustic pressure time-history at $(0, 0, 0)$ for setup 1: (———) theory; (−◯−) LBM simulation with 12 points per wavelength (DNS code).

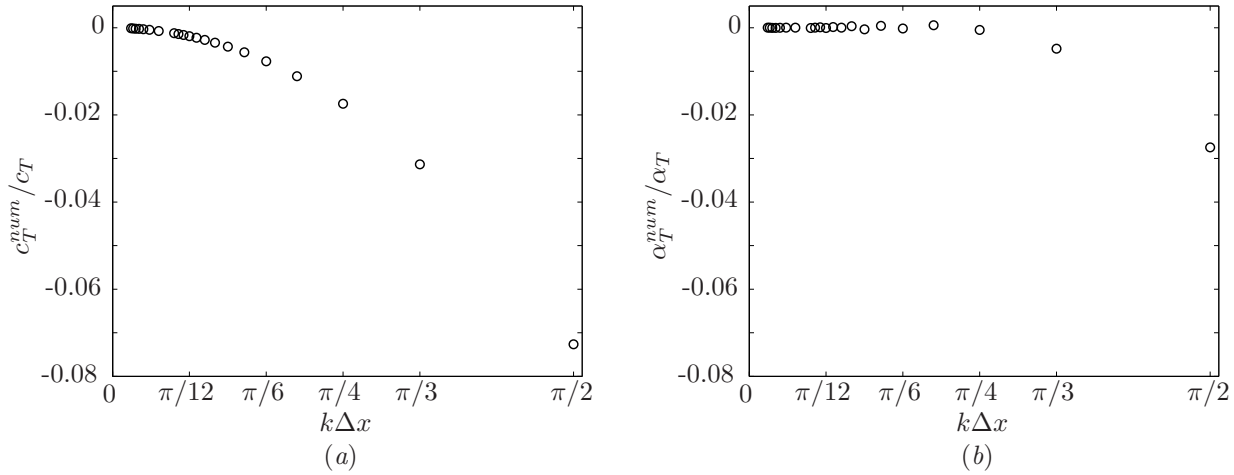

Figure 2. Relative numerical error for the setup 1 (DNS code) as a function of the nondimensional wavenumber $k\Delta x = 2\pi/N_{ppw}$: (a) phase speed; (b) dissipation rate.

Figures 2(a) and 2(b) show the relative numerical deviation of phase speed c_T^{num}/c_T and temporal dissipation rate α_T^{num}/α_T, respectively. Even at relatively low resolution with 12 points per wavelength (i.e., a nondimensional wavenumber $k\Delta x = \pi/6$), the deviation between the simulated and theoretical values is very small, about 0.77% on the phase speed and less than 0.02% on the dissipation rate.

These estimates are in excellent agreement with analytical and numerical results reported by Marié *et al.*.[19] Here, it is interesting to note that for simulations that are under-resolved, for instance with 4 points per wavelength, the ratio α_T^{num}/α_T is negative, meaning that the viscosity simulated is less than the expected value, and the shift in frequency can be significant (e.g., the measured frequency is $f \approx 9.3$ kHz instead of 10 kHz). The same trends are observed in reference 19.

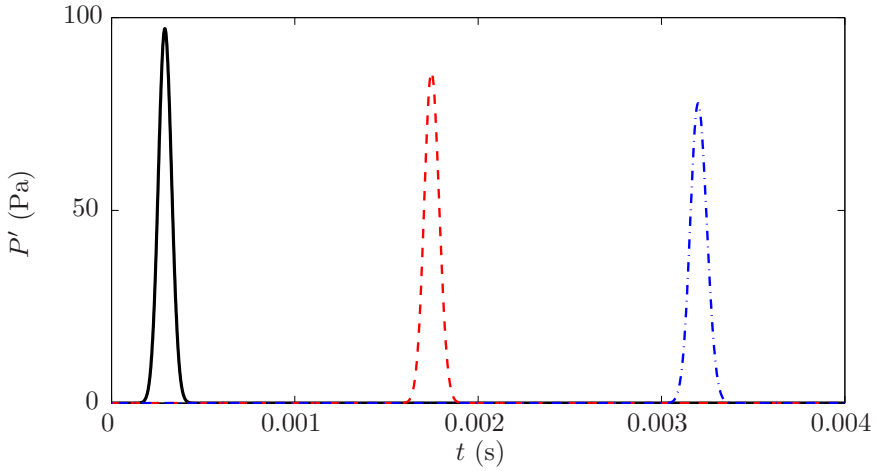

Figure 3. Acoustic pressure time-history for setup 2 (DNS code) with resolution $\Delta x = 0.001$ m: signal at reference probe (———); signal at 0.5 m (- - - -) and 1 m (—·—) from the reference probe.

Figure 3 shows the acoustic pressure time-history for the propagation of the planar Gaussian pulse, corresponding to setup 2, with a resolution $\Delta x = 0.001$ m. While various probe locations were considered, the time signal is only shown at the reference position, and after 0.5 m and 1 m of propagation. As expected, the loss in intensity measured at any location is directly proportional to the distance of propagation and the results are independent of the location of the measurements.

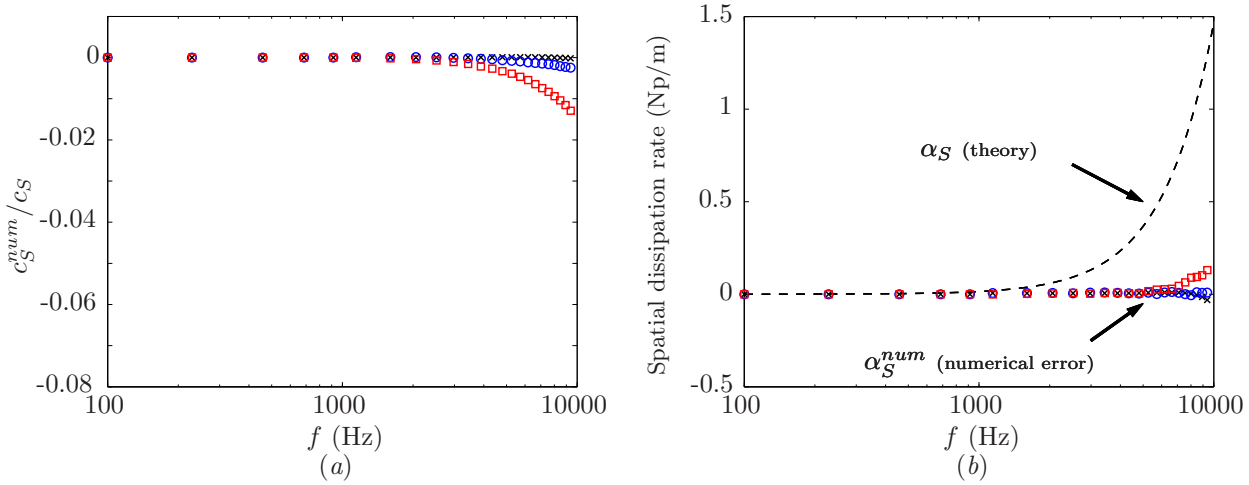

Figure 4. Relative numerical error for the setup 2 (DNS code) as a function of frequency for resolution $\Delta x = 0.001$ m (×), $\Delta x = 0.002$ m (○) and $\Delta x = 0.004$ m (□): (a) phase speed; (b) dissipation rate. The theoretical value of the dissipation rate is also shown by (- - - -).

Figures 4(a) and 4(b) show the relative numerical deviation of phase speed c_T^{num}/c_T, and the dissipation rates α_S^{num} in Np/m, where the neper (Np) is a dimensionless unit. Similarly to setup 1, these results show that numerical errors remain very small, that is the measured wave speed and decay rate match the expected physical values, even for the relatively low resolution (e.g., $\Delta x = 0.004$ m). Estimates of the intensity loss due to numerical dissipation can be obtained in dB/m from α_S^{num} in figure 4(b) and equation (10). For instance, a plane wave of frequency $f = 10$ kHz traveling on a mesh of resolution $\Delta x = 0.004$ m (i.e., with approximately 8 points per wavelength) will lose less than 1.5 dB per meter of propagation.

Overall, the results from the DNS version of the LBM code are in very good agreement with theoretical predictions, and show little numerical dispersion and dissipation. Similar conclusions were obtained in the

study by Lafitte and Pérot of the noise generated by cylinder flows,[30] where both the unsteady flow and the radiated pressure field were simulated directly using the DNS solver. Their results show good agreement both in term of aerodynamic and acoustic with various results from the literature. Our analysis also confirms the result from reference 17 that for the LBM-BGK isothermal model, the kinematic bulk viscosity has en effective value of $\nu_B = 2\nu/3$.

B. Turbulent code

Additional dissipation can be expected with the turbulent version of the LBM code because of added modeling in the simulation. To investigate these changes, the same simulations discussed earlier are performed, for setup 1 and 2, with the turbulence model on and the viscosity decreased to its value for air (e.g., $\nu = 1.5\ 10^{-5}$ m^2/s). The frequency range of interest is again within the human ear response. For such frequencies and low viscosity, the physical spatial absorptive loss is very small (e.g., $a_S \approx 0.01$ dB/m at $f = 10$ kHz), and the computed absorptive loss is then purely numerical.

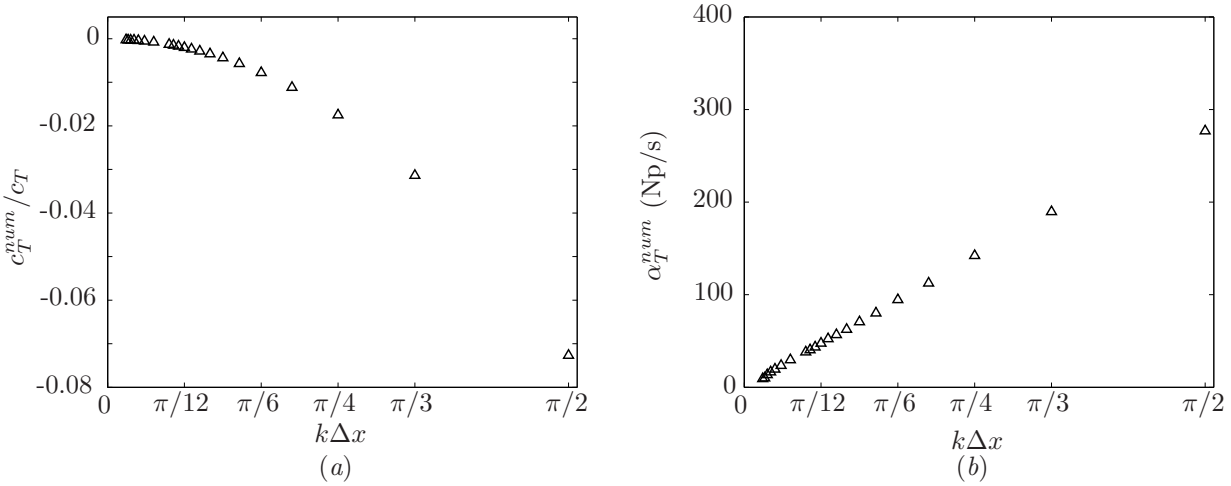

Figure 5. Relative numerical error for the setup 1 (turbulent code) as a function of the nondimensional wavenumber $k\Delta x = 2\pi/N_{ppw}$: (a) phase speed; (b) dissipation rate.

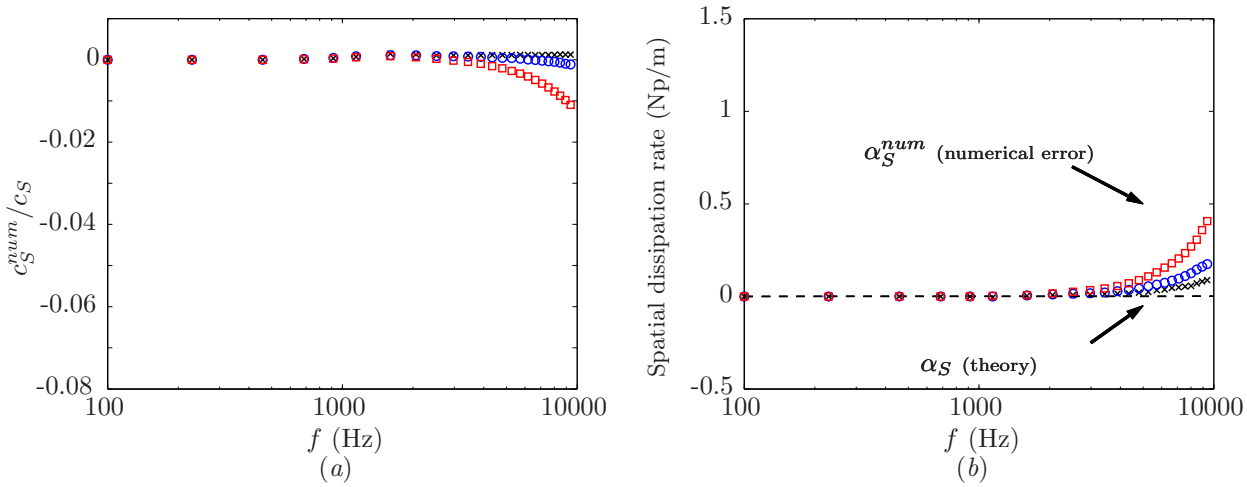

Figure 6. Relative numerical error for the setup 2 (turbulent code) as a function of frequency for resolution $\Delta x = 0.001$ m (×), $\Delta x = 0.002$ m (○) and $\Delta x = 0.004$ m (□): (a) phase speed; (b) dissipation rate. The theoretical value of the dissipation rate is also shown by (– – – –).

The results are presented in figures 5 and 6, for setup 1 (temporal analysis) and 2 (spatial analysis), respectively. First, it can be noticed that the deviation on the phase speed is almost identical to the previous results with the DNS code, that is the turbulence modeling does not introduce additional dispersion. In contrast, the numerical dissipation is larger in this case, and tends to scale inversely with resolution (or number of points per wavelength). This feature is clearly observed for the temporal dissipation rate in figure $5(b)$.

C. Guidelines on resolution requirements

For real-world engineering applications, one of the challenges of CAA is to balance computational cost and numerical accuracy. Typically, simulations are designed and setup with some maximum numerical dissipation allowed, depending on the particular length scales and frequencies of the problem (e.g., within 2 dB loss at the highest frequency of interest). In this section, different forms of the numerical absorptive loss are presented, yielding guidelines to estimate resolution requirement for practical applications.

The Gaster transformation in equations (11) and (12) is applied to the temporal dissipation rate α_T^{num} in figure $5(b)$. Multiplied by the fixed wavelength λ of the simulation, the absorptive loss from equation (10) can then be expressed as a loss in dB per wavelength of propagation, that is $a_\lambda = 8.7\lambda\alpha_T^{num}/c_0$. Here λ needs to be expressed in meters (i.e., the division of λ by 1 m is left unwritten in the nondimensionalization). The results are presented in figure 7 as a function of the number of points per wavelength N_{ppw}. A least square curve fitting shows an approximate $1/N_{ppw}$ dependency.

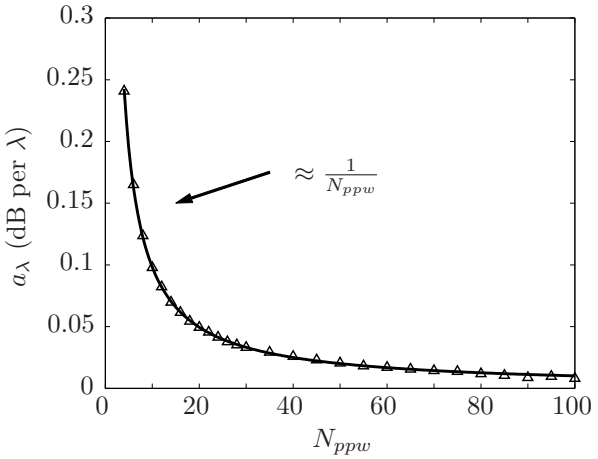

Figure 7. Numerical absorptive loss in dB per wavelength of propagation (△) for setup 1 (turbulent code) as a function of the number of points per wavelength N_{ppw}; A least square fitting estimate (———) is also shown.

A different form of the same result can be retrieved from the spatial dissipation rate in figure 6 (b). In this case, the absorptive loss from equation (10) is multiplied by the fixed resolution Δx of the simulation to obtain a loss in dB per cell of propagation, namely $a_{\Delta x} = 8.7\Delta x\alpha_S^{num}$. Like previously, the division of Δx by 1 m is left unwritten, and Δx needs to be in meters. The results are expressed as a function of the nondimensional frequency $f\Delta x/c_0$, which is simply $1/N_{ppw}$, the inverse of the number of points per wavelength. The set of curves in figure 6 then collapses into a single results shown in figure 8 (b). The least square curve fitting shows an approximate $1/N_{ppw}^2$ dependency, which is consistent with the previous results in figure 7, since wavelength and cell size are related by the number of points per wavelength (i.e., dB per λ = dB per Δx N_{ppw})

From figure 7, a choice of 12 to 16 points per wavelength leads to reasonable numerical losses, about 0.068 dB per wavelength of propagation. This would translate to less than 1 dB loss at 5 kHz and 1 m away. The same result can be obtained from figure 8: for $N_{ppw} = 14$ and the same frequency of 5 kHz, the nondimensional frequency is $f\Delta x/c_0 \approx 0.071$, and the loss per cell of propagation is 0.0046 dB, or 0.96 dB at 1 m.

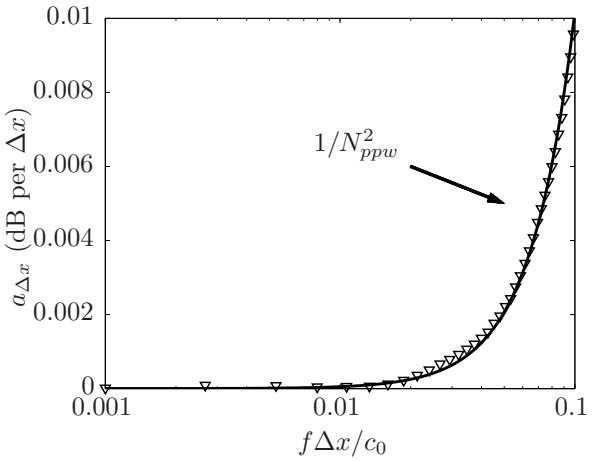

Figure 8. Numerical absorptive loss in dB per cell of propagation (▽) for setup 2 (turbulent code) as a function of the nondimensional frequency $f\Delta x/c_0 = 1/N_{ppw}$; A least square fitting estimate (———) is also shown.

V. Conclusions

In conclusion, good agreement was obtained between theoretical and numerical prediction for the propagation of acoustic waves, using the DNS version of the LBM code. Numerical dispersion and dissipation of the turbulent version of the LBM code was also investigated. The results show that the phase speed of the sound wave is essentially unaffected by the modeling, and that the method retains its low dispersive properties. Some additional numerical dissipation was observed and quantified. This analysis provides guidelines in terms of resolution in practical applications requiring the use of turbulence modeling, and could potentially be used to correct the noise levels for large propagation distances.

Overall, the results demonstrate the low dispersive and dissipative capabilities of the Lattice–Boltzmann method. For situations in which the propagation length scales of interest are of the order of a meter (e.g., vehicle interior noise), and the frequencies of interest are a few kHz, these results show the LBM is sufficiently accurate to achieve essentially no detrimental dissipation of sound energy in practical engineering problems.

References

[1]Qian, Y., d'Humieres, D., and Lallemand, P., "Lattice BGK models for Navier–Stokes Equation," *Europhys. Lett.*, Vol. 17(6), 1992, pp. 479–484.

[2]Chen, H., Teixeira, C., and Molvig, K., "Digital Physics Approach to ComputationalFluid Dynamics, Some Basic Theoretical Features," *Intl. J. Mod. phys. C*, Vol. 8(4), 1997, pp. 675.

[3]Shan, X., Yuan, X., and Chen, H., "Kinetic Theory Representation of Hydrodynamics: a way beyond the Navier–Stokes equation," *J. Fluid Mech.*, Vol. 550, 2006, pp. 413–441.

[4]Shock, R., Mallick, S., Chen, H., Yakhot, V., and Zhang, R., "Recent results on two-dimensional airfoils using a lattice Boltzmann-based algorithm," *J. Aircraft*, Vol. 39(3), 2002, pp. 434–439.

[5]Fares, E., "Unsteady Flow Simulation of the Ahmed Reference Body using a Lattice Boltzmann Approach," *Comput. Fluids*, Vol. 35(8-9), 2006, pp. 940–950.

[6]Vaillant, O. and Maillard, V., "Numerical Simulation of Wall Pressure Fluctuation on a Simplified Vehicle Shape," AIAA Paper 2003-3271, 2003.

[7]Senthooran, S., Crouse, B., G., B., Freed, D., Shin, S. R., and Ih, K. D., "Effect of Surface Mounted Microphones on Automobile Side Glass Pressure Fluctuations," Proc. 7th MIRA Intl. Vehicle Aerodynamics Conference, 2008.

[8]Pérot, F., Meskine, M., and Vergne, S., "Investigation of the Statistical Properties of Pressure Loadings on Real Automotive Side Glasses," AIAA Paper 2009-3402, 2009.

[9]Ricot, D., Maillard, V., and Bailly, C., "Numerical Simulation of the Unsteady Flow Past a Cavity and Application to Sunroof Buffeting," AIAA Paper 2001-2112, 2001.

[10]Crouse, B., Senthooran, S., Freed, D., Balasubramanian, G., Gleason, M., Puskarz, M., Lew, P., and Mongeau, L., "Experimental and Numerical Investigation of a Flow Induced Cavity Resonance with Application to Automobile Buffeting," AIAA Paper 2006-2494, 2006.

[11]Adam, J.-L., Ricot, D., Dubief, F., and Guy, C., "Aeroacoustic simulation of automobile ventilation outlets," JASA vol. 123, issue 5, p. 3250, 2008.

[12]Freeman, C. and Gaylard, A., "Integrating CFD and Experiment: The Jaguar Land Rover Aeroacoustics Process," Proc. 7th MIRA Intl. Vehicle Aerodynamics Conference, 2008.

[13]Balasubramanian, G., Crouse, B., and Freed, D., "Numerical Simulation of Real World Effects on Sunroof Buffeting of an Idealized Generic Vehicle," AIAA Paper 2009-3348, 2009.

[14]Keating, A., Beedy, J., and Shock, R., "Lattice Boltzmann Simulations of the DLR-F4, DLR-F6 and Variants," AIAA Paper 2008-749, 2008.

[15]Keating, A., Dethioux, P., Satti, R., Noelting, S., Louis, J., Van de Ven, T., and Vieito, R., "Computational Aeroacoustics Validation and Analysis of a Nose Landing Gear," AIAA Paper 2009-3154, 2009.

[16]Buick, J., Greated, C., and Campbell, D., "Lattice BGK Simulation of Sound Waves," *Europhys. Lett.*, Vol. 43(3), 1998, pp. 235–240.

[17]Dellar, P., "Bulk and Shear Viscosities in Lattice Boltzmann Equations," *Phys. Rev. E*, Vol. 64(3), 031203, 2001.

[18]Crouse, B., Freed, D., Balasubramanian, G., Senthooran, S., Lew, P., and Mongeau, L., "Fundamental Aeroacoustic Capabilities of the Lattice-Boltzmann Method," AIAA Paper 2006-2571, 2006.

[19]Marié, S., Ricot, D., and Sagaut, P., "Comparison between lattice Boltzmann method and Navier–Stokes high order schemes for computational aeroacoustics," *J. Comput. Phys.*, Vol. 228, 2009, pp. 1056–1070.

[20]Wolf-Gladrow, D., *Lattice-Gas Cellular Automata and Lattice Boltzmann Models*, Springler Verlag, Germany, 2000.

[21]Bhatnagar, P., Gross, E., and Krook, M., "A model for collision progresses in gases. I. small amplitude processes in charged and neutral one-component system," *Phys. Rev.*, Vol. 94(3), 1954, pp. 511–525.

[22]Chapman, S. and Cowling, T., *The Mathematical Theory of Non-Uniform Gases*, Cambridge University Press, 1990.

[23]Chen, H., Teixeira, C., and Molvig, K., "Realization of Fluid Boundary Conditions via Discrete Boltzmann Dynamics," *Intl. J. Mod. phys. C*, Vol. 9(8), 1998, pp. 1281.

[24]Chen, H., "Volumetric Formulation of the Lattice Boltzmann Method for Fluid Dynamics: Basic Concept," *Phys. Rev. E*, Vol. 58, 1998, pp. 3955–3963.

[25]Chen, S. and Doolen, G., "Lattice Boltzmann Method for Fluid Flows," *Ann. Rev. Fluid Mech.*, Vol. 30, 1998, pp. 329–364.

[26]Chen, H., Orszag, S., Staroselsky, I., and Succi, S., "Expanded Analogy between Boltzmann Kinetic Theory of Fluid and Turbulence," *J. Fluid Mech.*, Vol. 519, 2004, pp. 307–314.

[27]Kinsler, L. E., Frey, A. R., Coppens, A. B., and Sanders, J. V., *Fundamentals of acoustics*, John Wiley & Sons Inc., New York, 4th ed., 2000.

[28]Lamb, H., *Hydrodynamics*, Cambridge University Press, sixth ed., 1932.

[29]Gaster, M., "A note on the relation between temporally-increasing and spatially-increasing disturbances in hydrodynamic stability," *J. Fluid Mech.*, Vol. 14, 1962, pp. 222–224.

[30]Laffite, A. and Pérot, F., "Investigation of the Noise Generated by Cylinder Flows Using a Direct Lattice-Boltzmann Approach," AIAA Paper 2009-3268, 2009.